

Exchange Coupling in Magnetic Multilayers

M. D. Stiles

*Electron Physics Group, National Institute of Standards and Technology,
Gaithersburg MD 20899-8412*

Abstract

In magnetic multilayers, the magnetizations of two ferromagnetic layers separated by a non-magnetic spacer layer are coupled by the electrons in the spacer layer. This coupling oscillates in sign as a function of the thickness of the spacer layer. Extensive research done on these systems has led to a simple model for this coupling and remarkable agreement between predictions of the model and measurements of the coupling. The model predicts that the periods of the coupling are determined by geometrical properties of the Fermi surface belonging to the spacer layer material. The oscillatory coupling is an instance of oscillations in metals caused by the existence of a Fermi surface.

Key words: magnetic multilayers, exchange coupling, quantum well, spin-dependent reflection, Fermi surface, biquadratic coupling, critical spanning vector, interface electronic structure

PACS: 73.21.Ac, 75.30.Et, 75.70.Cn, 73.20.At, 72.25.Ba, 71.18.+y

1 Introduction

Varying the thickness of a layer separating two magnetic layers can give rise to dramatic oscillations in the magnetic coupling between them. A magnetic multilayer consists of a sequence of thin films grown on top of each other, each film ranging in thickness from tenths of nanometers to tens of nanometers. Typically, two thin films of ferromagnetic material are separated from each other by a thin film of a non-magnetic material, referred to as a spacer layer. The magnetization directions of the ferromagnetic layers are coupled to each other through an exchange interaction. The sign of this coupling oscillates as the thickness of the spacer layer is varied, with the best multilayer samples showing up to thirty periods of oscillation. This chapter gives a pedagogical

Email address: `mark.stiles@nist.gov` (M. D. Stiles).

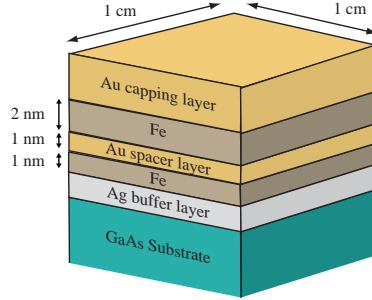


Fig. 1. Typical magnetic multilayer. Here two Fe layers are separated by an Au spacer layer. An Au capping is grown on top to protect the multilayer from corrosion. The multilayer was grown on a GaAs substrate with a buffer layer of Ag to promote better growth of the Fe and Au films.

description of the origin of the coupling and describes a few key measurements and calculations.

In metals, the sharp cut-off in occupancy at the Fermi surface causes oscillatory phenomena. The oscillation of the induced magnetization as a function of applied magnetic field, called the de Haas-van Alphen effect [1], is a well known example. Many other properties oscillate as well. These oscillations arise from field induced oscillations in the density of states. The cross-sectional areas of the Fermi surface, a geometrical property, determine the oscillation periods.

Spatially localized disturbances in metals lead to another type of oscillation. The oscillation of the electron density near surfaces of metals, known as Friedel oscillations, is an example. Another example is the oscillation in the interaction between two localized magnetic impurities in a metallic host. As the separation between the impurities is increased, the interaction between them oscillates between favoring parallel alignment and antiparallel alignment of the magnetic moments. This coupling of the moments is known as the Ruderman-Kittel-Kasuya-Yosida (RKKY) interaction [2]. A different geometrical property of the Fermi surface determines the spatial periods of the oscillations between the localized disturbances, in this case, a vector spanning the Fermi surface from one side to the other. Interlayer exchange coupling is a particularly dramatic instance of this type of oscillation.

Observation of coupling in magnetic multilayers requires high quality thin films. Early studies [3] were plagued by a number of extrinsic sources of coupling due to defects. One source of such coupling is the presence of pinholes, regions where the non-magnetic layer was not continuous. Pinholes give direct contact between the ferromagnetic layers, leading to coupling favoring parallel alignment of the magnetization directions, referred to as ferromagnetic coupling. In addition, correlated roughness of the films causes ferromagnetic “orange peel” coupling [4]. In 1986, Grünberg [5] demonstrated antiferromagnetic coupling between the magnetizations of two Fe layers separated by Cr

and two groups demonstrated coupling in rare earth multilayers [6,7]. The observation of antiparallel alignment of the magnetizations meant that the magnetic layers had been grown well enough that the coupling due to any extrinsic coupling was much smaller than the intrinsic coupling.

Once high quality multilayers could be grown, interest in them started to explode. Two years later, Grünberg's group and Fert's group discovered the Giant Magnetoresistance (GMR) effect [8,9]. Magnetoresistance refers to the dependence of a sample's resistivity on an applied magnetic field. The field dependence may be indirect, for example the resistance can depend on the magnetization direction, which can depend on the applied field. This is true for giant magnetoresistance; the resistance depends on the relative orientation of the magnetizations of the ferromagnetic layers. If the magnetizations of two layers are antiparallel for zero applied field because the layers are antiferromagnetically coupled, an applied field can overcome the coupling and bring the films into parallel alignment. This change in alignment leads to a change in resistance – giant magnetoresistance.

It was immediately realized that the giant magnetoresistance effect could be a sensitive magnetic field detector, particularly for read heads in magnetic disk drives. In fact, read heads based on the giant magnetoresistance effect are now used in essentially all disk drives. To optimize the performance of the read heads, magnetic multilayers with different materials, layer thickness, growth conditions, and other parameters were studied. In 1990 [10], Parkin discovered oscillatory behavior of the dependence of the giant magnetoresistance on the thickness of the non-magnetic spacer layer. These oscillations were not due to variations in the transport properties, but rather variations in the coupling between the ferromagnetic layers. For some thicknesses the coupling was ferromagnetic, favoring parallel alignment of the magnetization directions. For these thicknesses, there was no change in the relative alignment of the magnetizations when a magnetic field was applied and hence the magnetoresistance was zero.

The oscillations in the coupling as a function of the separation between two magnetic objects immediately brought to mind the RKKY interaction between magnetic impurities. There was one big puzzle however. The oscillation period, approximately 1.0 nm, was much longer than was expected from estimates based on the analogy with the RKKY interaction. The answer to the puzzle, as is described in detail below, is that it is possible to make much more quantitative comparisons between theory and experiment for magnetic multilayers than has been done for magnetic impurities. The rest of this article is devoted to describing what goes into this comparison.

In the following section, I describe a simple model for the physics of the inter-layer exchange coupling. Despite its simplicity, this model allows quantitative

comparison between theory and experiment. I give this comparison as well as a comparison with more sophisticated models. Section 3 describes the experimental techniques that are used to prepare magnetic multilayers, characterize them, and measure the coupling. I discuss how the presence of defects affects the comparison between theory and experiment. Not only do these defects modify the interlayer exchange coupling, but they can also create effective couplings with different forms. Section 4 describes the most common such effective interaction – biquadratic coupling.

2 Quantum Well Model

2.1 Model for Transition Metal Ferromagnetism

Developing a simple model for interlayer exchange coupling requires starting with a simple model for the electronic structure of ferromagnets. Unfortunately the electronic structure of transition metal ferromagnets is quite complicated. Ferromagnetism in transition metals is driven by atomic-like exchange and correlation effects in the partially filled d -electron shells. The atomic-like effects suggest a localized description of this part of the electronic structure. However, the d orbitals are strongly hybridized with d orbitals on neighboring atoms and also with the s - p orbitals on neighboring atoms. The strong hybridization suggests an itinerant description of the electronic structure. Reconciling these aspects of the physics is an ongoing area of research, and the resulting models are not simple [11]. Simplifying the model requires approximations that favor one aspect of the physics over the other. In this article, I adopt a description favoring the itinerant aspects because the interlayer exchange coupling depends strongly on the properties of the electrons at the Fermi surface and a realistic description of the Fermi surface requires treating the itinerant nature of the d electrons.

The local-spin-density approximation (LSDA) [12] accurately describes the itinerant aspects of the electronic structure while treating the atomic-like exchange and correlation effects in mean field theory. That is, all of the complicated electron-electron interactions are lumped into a local potential that depends on the local density and the local spin density. This approximation was derived for computing the ground state properties of materials. For transition metal ferromagnets, it works quite accurately for properties like the cohesive energy, equilibrium lattice constant, and the magnetic moment [13]. Formally, it is not justified for computing the electronic structure, but it is a good combination of simplicity and accuracy even for this case.

A material becomes ferromagnetic when it is energetically favorable for a ma-

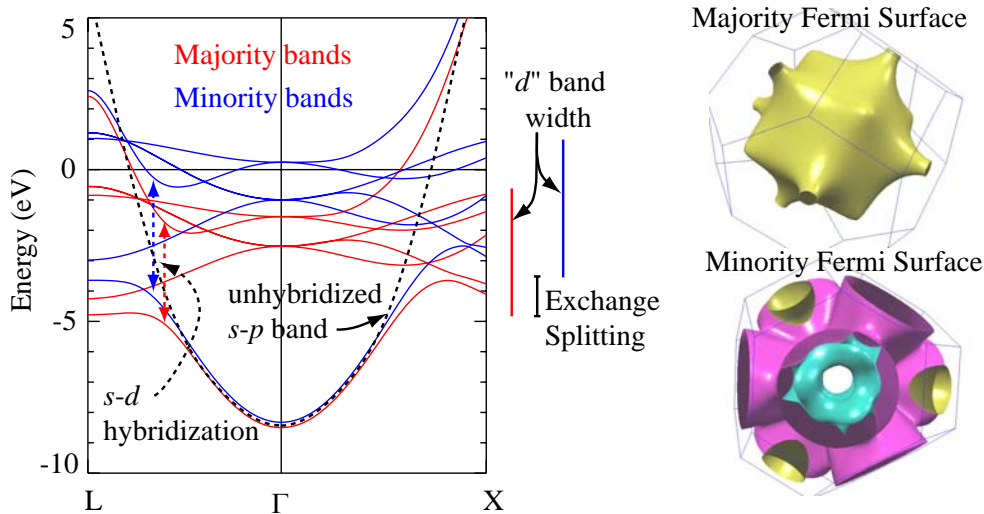


Fig. 2. The band structure and Fermi surface of face-centered cubic Co. The red (blue) curves give the majority (minority) bands along two high symmetry directions through the Brillouin zone center, Γ . The dotted black curve shows the s - p band if it were not hybridized with the d bands. The bars to the right of the bands show the width of the d bands and the shift between the majority and minority bands. The red and blue arrows in the band structure plots give the width of the gap due to the hybridization between the s - p and d bands of the same symmetry along the chosen directions. The Fermi surfaces are by permission from Choy et al., [14].

majority of electrons to align their spins parallel to one another. The electrons then split into those with spins parallel to the majority of the other spins (majority) and those antiparallel (minority). Spin-orbit coupling mixes these states, but is weak enough to ignore to a first approximation. Ignoring the spin-orbit coupling leads to a description of ferromagnets in terms of two separate sets of electrons, majority and minority, which have different properties. This description also holds in the non-magnetic layers in magnetic multilayers provided the magnetizations in the different ferromagnetic layers are all collinear with each other. When the magnetizations are not collinear, spin currents flow in the non-magnetic layers and exert torques on the ferromagnetic layers, as is described below.

Figure 2 shows a band structure for Co in a face-centered cubic (fcc) structure calculated using the LSDA, highlighting the importance of the itinerant aspects of the electronic structure. The d -bands have a width in energy, approximately 5 eV, that is large compared to the exchange splitting between the majority and minority bands, about 2 eV. In addition, The hybridization between the d -bands and the s - p band is large enough to lead to a gap of about 3 eV where the bands would cross if they were not hybridized. Finally, Fig. 2 shows images of the Fermi surface for majority and minority electrons. Clearly, these are quite different, and the two sets of electrons have very different properties.

There are two simplified models for the electronic structure of ferromagnets that have been used extensively in studies of magnetic multilayers. Each emphasizes different aspects. Both include free-electron-like bands. In the spin-split free electron model, the free-electron-like bands for majority and minority electrons are shifted in energy relative to each other by a constant exchange shift. This model ignores the d electrons completely, but the Fermi surfaces for majority and minority electrons are different. I use this model for pedagogical purposes in much of the rest of this section.

The other model, called the s - d model, emphasizes the atomic like aspects of the d -orbitals by ignoring the d - d hybridization and treating the orbitals as completely localized. This model was originally used to treat isolated magnetic impurities in a non-magnetic host. For ferromagnets and magnetic multilayers, the model for isolated impurities is generalized to treat a dense set of such impurities. In this model, the s - p electrons are weakly hybridized with the d -electrons. In some limits it is possible to map the s - d model onto a local moment model in which the d -electrons form a local moment with a fixed total spin \vec{S}_i , where i labels the site. The hybridization between the d and s electrons becomes an exchange interaction between the local moment and the s - p electron spin $\vec{\sigma}$ with the form $-J\vec{S}_i \cdot \vec{\sigma}$. The s - d model and the local moment model have been used both to study interlayer exchange coupling and extensively to study transport in magnetic multilayers, i.e. the giant magnetoresistance, see the chapter by Fert in this volume. As long as the scattering rates for minority and majority electrons are different, these models capture much of the essential physics. However, care must be taken when the details of the band structure are important.

2.2 Spin Polarized Quantum Well States

In this section, I describe the properties of a magnetic multilayer using a spin-split free electron model as described above [15]. In this model, interfaces are simply potential steps. Below, I generalize the results to more realistic models of the electronic structure.

An interface between two materials acts on the electrons like a potential step; electrons that strike it have a transmission probability reduced from one. For a free electron going down a simple potential step of height V the transmission probability is

$$T_{\text{step}} = \frac{q}{k} \left(\frac{2k}{k+q} \right)^2. \quad (1)$$

Here, the incident wave vector is $k = \sqrt{2mE/\hbar^2}$ and the transmitted wave

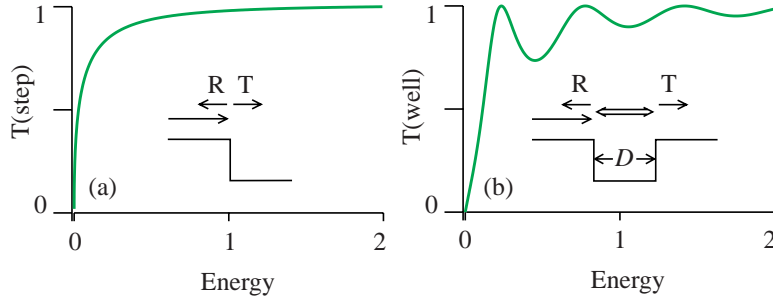


Fig. 3. Electron transmission probabilities for a step and a quantum well.

vector is $q = \sqrt{2m(E + V)/\hbar^2}$. The first factor accounts for the change in velocity on going over the step. The transmission probability is plotted in Fig. 3(a).

If another step is introduced, the electron undergoes multiple reflection inside the quantum well that is formed (see Fig. 3(b)). If the steps are separated by a distance D , the transmission probability is

$$T_{\text{well}} = \left| \frac{4e^{iqD}kq}{(k+q)^2 - e^{i2qD}(k-q)^2} \right|^2. \quad (2)$$

Note that the transmission probability goes to one whenever $2qD = 2n\pi$, where n is an integer. At a fixed thickness, there is a series of transmission resonances at the energies $E_n = 2m\hbar^2(n\pi/D)^2 - V$, for integer n . At a fixed energy, there are resonances for $D = 2n/(\pi 2q)$ with $q = \sqrt{2m(E - V)/\hbar^2}$; these resonances are separated by a fixed increment in thickness. At the transmission resonances, the electrons have an increased probability to be in the quantum well, in other words, there is a peak in the density of states in the quantum well at the energy of the resonance.

These peaks in the density of states are seen in magnetic multilayers using photoemission and inverse photoemission, for reviews see [16–19]. Photoemission is a technique in which photons of a particular energy, generally ultraviolet light or x-rays, are incident on a surface. When the photons are absorbed by the material, they excite electrons which can leave the surface and be measured. The energy of the electron in the solid can be inferred from the photon energy and the energy of the photoemitted electron. Peaks are observed in the photoemission spectrum where there is a large density of states in the material.

Photoemission probes the near surface region because the escape depth of the photoemitted electrons is on the order of a nanometer. In order to see the density of states peaks in the non-magnetic spacer layer, the top magnetic layer needs to be stripped off (or never deposited in the first place). In other words

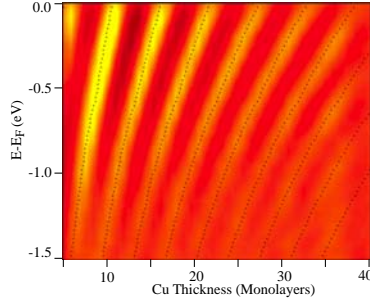


Fig. 4. Photoemission from a Cu overlayer on Co. Yellow indicates high photoemission intensity and red low intensity. Reproduced with permission from Z. Qiu [19]

the quantum well states studied in photoemission are not exactly the same quantum well states that are present in the complete magnetic multilayer. None the less, there is very good correspondence between these states and the related states in magnetic multilayers. Figure 4 shows the photoemission intensity as a function of energy and spacer layer thickness. This figure shows the fixed spacing between peaks as a function of thickness and the quadratic variation of the peaks as a function of energy. There are some differences between what would be expected for a free electron model and what is observed.

To understand how the free electron model generalizes to real materials it is instructive to rewrite the transmission probability in terms of the transmission probability for a step and the reflection *amplitude* at an isolated step $R = (k - q)/(k + q)$. This substitution emphasizes the contribution made by multiple reflection inside the quantum well. One round trip through the well has the amplitude $e^{i2qD} R^2$ from reflecting from each step and propagating both directions through the well. The transmission probability is

$$T_{\text{well}} = \left| T_{\text{step}} e^{iqD} \frac{1}{1 - e^{i2qD} R^2} \right|^2 = \left| T_{\text{step}} e^{iqD} \sum_{n=0}^{\infty} (e^{i2qD} R^2)^n \right|^2. \quad (3)$$

The second form shows explicitly the coherent multiple scattering in the well. The basic physics of quantum well states in real materials is captured by replacing the wavevector for propagating through the spacer layer, q , by the appropriate value from the real band structure and by replacing the reflection amplitude and transmission probability by the values calculated for a realistic interface.

If one of the materials is ferromagnetic, the potential step for the majority and minority electrons is different. In a multilayer with two magnetic layers there are four possible quantum wells formed depending on the relative alignment of the magnetizations, see Fig. 5. The quantum well states for each of these are different because the potential steps, and hence reflection probability, is

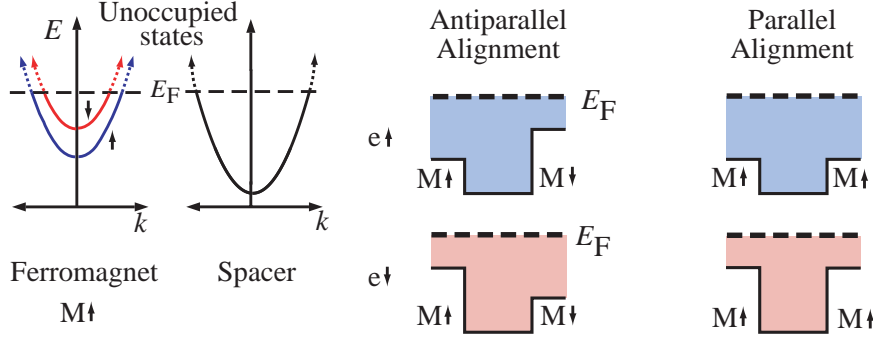


Fig. 5. Quantum wells used to compute interlayer exchange coupling. On the left, the two panels give typical band structures for free electron models of interlayer exchange coupling. On the right, the four panels give the quantum wells for spin up and spin down electrons for parallel and antiparallel alignment of the magnetization. The shaded regions designate the occupied states.

different for each quantum well. However, at a particular energy, like the Fermi energy, the quantum well states in all of the wells have the same periodicity as a function of the thickness of the spacer layer, because the periodicity only depends on the wave length of the electron in the spacer layer at that energy.

2.3 Interlayer Exchange Coupling

The interlayer exchange coupling can be described in terms of an energy that depends on the magnetization directions of the two layers, \hat{m}_i

$$E = -JA\hat{m}_1 \cdot \hat{m}_2 , \quad (4)$$

where A is the area of the two films, and $J < 0$ gives antiferromagnetic coupling favoring antiparallel alignment. The form of the coupling is called bilinear in contrast the biquadratic coupling described in Sec. 4. For interlayer exchange coupling of the form given in Eq. (4) the strength of the exchange interaction is determined by the difference in energy between the quantum well with parallel magnetizations and that with antiparallel magnetizations. Computing the exchange interaction simply requires computing the energies of the quantum wells given in Fig. 5. For large spacer layer thicknesses, the result is

$$\begin{aligned} J &= \frac{\hbar v_F}{2\pi D} \text{Re} \left[(R_\uparrow R_\uparrow + R_\downarrow R_\downarrow - R_\uparrow R_\downarrow - R_\downarrow R_\uparrow) e^{i2k_F D} \right] + O(D^{-2}) \\ &\approx \frac{\hbar v_F}{2\pi D} |R_\uparrow - R_\downarrow|^2 \cos(2k_F D + \phi) . \end{aligned} \quad (5)$$

Here, k_F is the Fermi wave vector in the spacer layer, $v_F = \hbar k_F / m_e$ is the Fermi velocity, m_e is the electron mass, and R_\uparrow and R_\downarrow are the reflection amplitudes for a majority and minority electron to reflect from the interface. Expanding the square of the reflection amplitudes gives four terms, one for each of the quantum wells in Fig. 5. The exchange coupling oscillates in sign with a period π/k_F , the oscillation decays like D^{-1} , and the amplitude of the oscillation is determined by the spin dependence of the reflection amplitudes.

Physically these oscillations arise because the quantum well resonances cross through the Fermi level as the thickness of the spacer layer is increased, see Fig. 4. Each time the thickness increases by π/k_F another resonance crosses through the Fermi level. The resonances for each of the quantum wells in Fig. 5 are all different, but they all have the same period because the period is determined by the Fermi wavevector in the spacer layer, and is independent of the properties of the magnetic material.

2.3.1 Critical spanning vectors

The expression for the interlayer exchange coupling, Eq. (5), is based on a one dimensional model. Generalizing to realistic three-dimensional systems is straightforward if the growth of the multilayer is *coherent*. For coherent growth, the in-plane lattice of all of the layers is the same, so the in-plane momentum (wave vector) is conserved when the electrons scatter from the interfaces. In this case, electrons with different values of in-plane wave vector do not couple, so the quantum well states for different in-plane wave vectors are independent of each other. Including the full three dimensions of the multilayer then simply requires integrating the one-dimensional result over the in-plane wave vector

$$\frac{J}{A} = \frac{\hbar}{2\pi D} \int \frac{d^2 K}{(2\pi)^2} v_F(\vec{K}) \text{Re} \left[(R_\uparrow(\vec{K}) - R_\downarrow(\vec{K}))^2 e^{i2k_z(\vec{K})D} \right] + O(D^{-3}) . \quad (6)$$

This integral is simple in the limit of large D ; there is a contribution whenever the spacer layer spanning vector, $2k_z(\vec{K})$, is constant as a function of \vec{K} . The vector connecting one sheet of the Fermi surface to another at this in-plane wave vector is called a critical spanning vector. In general, the oscillating contributions from different parts of the Fermi surface are out of phase and tend to cancel each other. However, when the spacer layer spanning vector is constant as a function of \vec{K} , the contributions from finite region of the Fermi surface near the critical point are in phase. This region gives a contribution to the integral that oscillates in thickness with a period determined by the critical spanning vector. As the thickness D becomes larger, the region of the Fermi surface that contributes in phase gets smaller so that the amplitude of the oscillation decreases with an additional power of D .

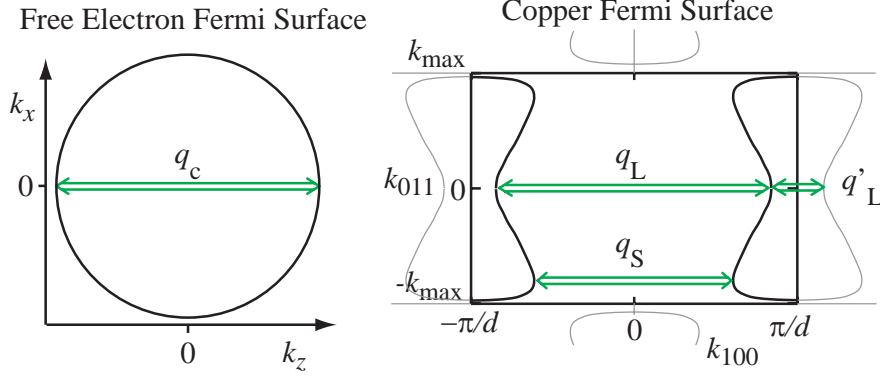


Fig. 6. Slices through a free electron and the Cu Fermi surfaces. For the spherical free electron Fermi surface, there is one critical spanning vector $q_c = 2k_F$. For the Cu Fermi surface, there are two inequivalent critical spanning vectors, q_L which is closely related to the free electron critical spanning vector, and q_S which occurs in the necks of the Fermi surface. The Cu Fermi surface is shown within the Brillouin zone appropriate for Cu(001) multilayers. Indicated in gray are parts of the Fermi surface in the extended zone scheme. The critical spanning vector q'_L is equivalent to q_L because of the discrete nature of the lattice.

For free electrons, the critical spanning vector is $q_{\text{crit}} = 2k_F$, the vector that goes from one side of the sphere to the other, see Fig. 6. For a free electron model, the interlayer exchange coupling is

$$\frac{J}{A} = -\frac{\hbar v_F k_F}{16\pi^2 D^2} \left[R_{\uparrow}(\vec{0}) - R_{\downarrow}(\vec{0}) \right]^2 \sin(2k_F D) + O(D^{-3}). \quad (7)$$

The in-plane wave vector dependence of the Fermi velocity and the reflection amplitudes is ignored to lowest order. The oscillation period only depends on the geometry of the spacer layer Fermi surface, but the strength of the oscillation depends on the Fermi surface through v_F and k_F and also the details of the electronic structure of the ferromagnet through R_{\uparrow} and R_{\downarrow} .

The generalization to realistic materials is illustrated for Cu in Fig. 6. For a free electron model, the only critical spanning vector is one of length $2k_F$ connecting one side of the Fermi sphere to the other. However, for realistic materials, the Fermi surface is more complicated than a sphere; in general there are several critical spanning vectors and there is a contribution to the coupling from each. For thick spacer layers, the coupling is

$$J(D) = \sum_{\alpha} \frac{\hbar v_{\perp}^{\alpha} \kappa^{\alpha}}{16\pi^2 D^2} \text{Re} \left[(R_{\uparrow}^{\alpha} - R_{\downarrow}^{\alpha})^2 e^{iq_{\perp}^{\alpha} D} e^{i\chi^{\alpha}} \right] + O(D^{-3}). \quad (8)$$

For each critical point, q_{\perp}^{α} is the critical spanning vector, v_{\perp}^{α} is the Fermi velocity, κ^{α} is the average radius of curvature of the Fermi surface, and $e^{i\chi^{\alpha}}$ is a phase that depends on whether the stationary point is a minimum, maximum

Table 1

Comparison of oscillation periods measured in magnetic multilayers with those expected from the critical spanning extracted from Fermi surfaces measured in de Haas-van Alphen measurements (dHvA).

Interface	Period (ML)	Period (ML)	Technique	Reference
Ag/Fe(100)	5.58	2.38	dHvA	[21]
	5.73 ± 0.05	2.37 ± 0.07	SEMPA	[22]
Au/Fe(100)	8.60	2.51	dHvA	[21]
	8.6 ± 0.3	2.48 ± 0.05	SEMPA	[23]
Cu/Co(100)	5.88	2.56	dHvA	[21]
	8.0 ± 0.5	2.60 ± 0.05	MOKE	[24]
	6.0 to 6.17	2.58 to 2.77	SEMPA	[25]
Cr/Fe(100)	11.1		dHvA	[26,27]
	12 ± 1		SEMPA	[28]
	12.5		MOKE	[29]
Cr/Fe(112)	14.4		dHvA	[26]
	15.4		MOKE	[29]

or saddle point. Eq. (8) is known as the asymptotic formula. It is valid for thick spacer layers; for thinner spacer layers, the $O(D^{-3})$ represents preasymptotic corrections.

Equation (8) shows that the oscillation periods observed in interlayer exchange coupling are determined by geometrical properties of the spacer layer Fermi surface. The first paragraph of this chapter mentioned that the de Haas-van Alphen effect measures the geometry of the Fermi surface. In 1991, Edwards et al. [20] pointed out the analogy between the oscillations in the interlayer exchange coupling and the oscillations seen in the de Haas-van Alphen effect. Also in 1991, Bruno and Chappert [21] showed that it was possible to use the Fermi surfaces determined in de Haas-van Alphen measurements to predict the periods that would be observed in measurements of magnetic multilayers. Table 1 shows the resulting comparison. The agreement between the two sets of periods is quite remarkable. I describe the experimental techniques used to measure the interlayer exchange coupling periods in the next section and discuss some of the possible reasons for the disagreement seen for Cu/Co(100).

It is interesting to note that the oscillations in the interlayer exchange coupling and in the de Haas-van Alphen effect come from different critical features of the Fermi surface. In both cases, the oscillations are due to the abrupt change

in occupancy at the Fermi energy. In the case of interlayer exchange coupling, there are oscillatory contributions to the coupling at all the energies and in-plane wave vectors of the occupied states. However, all of these oscillations tend to cancel out, except where the occupancy changes at the Fermi surface. Further, the oscillations at the Fermi surface all cancel except at points where two sheets of the Fermi surface become parallel to each other. There are similar oscillations in the de Haas-van Alphen effect. These also all cancel except at the Fermi energy and where the area of the orbit in reciprocal space is stationary as a function of the wave vector along the magnetic field direction.

In this respect, these oscillatory phenomena are physical examples of a simple mathematical effect. In a Fourier transform, a function is described as a superposition of oscillating functions with different frequencies. An approximate description results when the range of frequencies is finite, i.e. when there is an upper cut-off frequency. Whenever the function being described has a sharp feature, a kink or a step for example, approximate descriptions with a finite cut-off oscillate close to the location of the sharp feature. These oscillations are known as Gibbs oscillations. For the interlayer exchange coupling and the de Haas van Alphen effect, the sharp cut-off is the Fermi surface where the occupancy changes from one to zero.

Another interesting comparison of the two sets of oscillations is found in the different conditions that are required to observe both. The de Haas-van Alphen oscillations come about when electrons in a magnetic field complete a circular orbit before they scatter. For typical fields, these orbits are large, requiring long mean free paths, that is, low temperatures and very high quality crystals. As shown above, interlayer exchange coupling requires that electrons complete a round trip within the spacer layer before scattering. This path is much shorter than that required for de Haas-van Alphen oscillations, consistent with the fact that oscillatory interlayer exchange coupling is observed at temperatures even higher than room temperature. Even though the interlayer exchange coupling is less sensitive to the mean free path, it was discovered much later because growing sufficiently good multilayers requires deposition techniques that has only recently been developed.

Figure 6 illustrates the resolution to the early doubts that interlayer exchange coupling was related to the RKKY interaction. These doubts were driven by the fact that the period expected from the free electron critical spanning vector is close to 0.3 nm, which is much shorter than the observed period of about 1.0 nm. Taking the actual Fermi surface into account does not immediately help. The Cu Fermi surface is a distorted sphere and the critical spanning vector q_L is close to the free electron $2k_F$. The resolution of this discrepancy derives from the fact that Cu has a periodic lattice and in multilayers has layers of thickness d . Hence, the coupling can only be sampled at discrete values of the thickness nd for integer n . Since the oscillation corresponding

to the free electron Fermi surface has a period shorter than d , the oscillation with wave vector q_L is indistinguishable from an oscillation with wave vector $q'_L = (2\pi/d) - q_L$. The period associated with q'_L is very close to what is seen experimentally. The equivalence of a discretely sampled rapid oscillation to a slower oscillation is referred to as *aliasing*.

Aliasing is the reason that the Cu(100) critical spanning vectors are labeled the way they are in Fig. 6. The longer critical spanning vector q_L gives a longer period oscillation than the shorter critical spanning vector q_S gives. Without aliasing, it would be the other way around.

2.3.2 Coupling Strength

While the critical spanning vectors and other properties of the Fermi surface in Eq. (8) can be extracted from experiment, the reflection amplitudes cannot. For real multilayers, these can be calculated, but the resulting coupling strengths do not agree nearly as well with measured values as the periods do. Some of the disagreement is due to experimental difficulties, which are discussed in the next section, but some disagreement is due to theoretical difficulties.

The asymptotic form is an approximation to the difference in energy between the total energies of multilayers with parallel magnetizations and antiparallel magnetizations. Unfortunately, due to the complexities of the electron-electron interaction, it is currently impossible to compute these total energies without approximation. The best available approximation, as described in the beginning of this section, is the local spin density approximation (LSDA). This approximation works quite well for magnetic multilayers but with one caveat. The band structure is only approximate, so the Fermi surface deviates from its actual shape. Since the oscillation periods of the interlayer exchange coupling depend on the critical spanning vectors of the spacer layer Fermi surface, the periods computed using the LSDA will be wrong. This means that after a few oscillations, the calculated coupling is out of phase with the experimental coupling. The sign of the coupling may even be wrong. A direct comparison is then misleading because even if the physics is essentially correct, the agreement might be quite poor, see Fig. 7. There, the agreement is made even worse by the effect of disorder on the measured results.

In Fig. 7, the calculated and measured periods of the oscillations disagree; the periods extracted from the experiment are 2.48 ± 0.05 monolayers and 8.6 ± 0.3 monolayers and the critical spanning vectors of the theoretical Fermi surface would give periods of 2.65 monolayers and 8.03 monolayers. One way to compensate for the errors in the periods is to fit both theory and experiment to the asymptotic form, and compare the envelopes. The results of fits

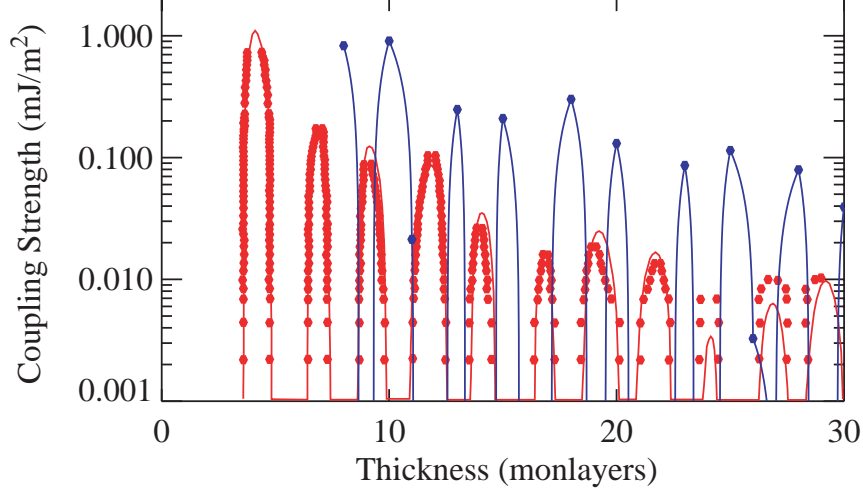


Fig. 7. Calculated [30] and measured [31] coupling strengths for Fe/Au/Fe(100) multilayers. The red (blue) symbols are the measured (calculated) coupling strengths. The red curve is the best fit to the experimental data when the measured thickness fluctuations are taken into account. The blue curve is a linear interpolation between the coupling strengths calculated for complete layers.

Table 2

Comparison of coupling strengths.

	$J^S/(1 \text{ nm})^2$	$J^L/(1 \text{ nm})^2$
Fit to experiment [31]	$1.29 \pm 0.16 \text{ mJ/m}^2$	$0.18 \pm 0.02 \text{ mJ/m}^2$
Asymptotic Calculation [34]	2.0 mJ/m^2	1.1 mJ/m^2
Fit to Full Calculation [30]	3.4 mJ/m^2	1.1 mJ/m^2

to the calculations and measurements in Fig. 7 are given in Table 2. The fits to experiment take into account measured thickness fluctuations, as discussed in the next section. Taking into account the thickness fluctuations leads to much better agreement between the strengths in Table 2 than in the raw comparison in Fig. 7. An additional source of disagreement that has not been accounted for is temperature. The calculations are done at zero temperature and the measurements at room temperature. While it is clear that accounting for the temperature will improve the comparison, the temperature scale for the correction [32,33] in this system is not known so it cannot be made quantitative. Measuring the coupling at low temperature would be the ideal solution. Possible reasons for any remaining disagreement are discussed in the next section. Also given in Table 2 are calculations done using the asymptotic form. Possible reasons for the imperfect agreement between calculations are discussed below.

A difficulty with total energy calculations is that the total energies are typically many orders of magnitude larger than the difference in energy between

parallel and antiparallel alignment of the magnetizations. In the LSDA, the density and the potential depend on each other and need to be determined self-consistently. Accurately computing energy differences makes the calculations quite time consuming. One way to simplify the process is to use the force theorem. The force theorem states that if the densities (or potentials) of two configurations are close to each other, the difference in total energies can be approximated by the difference in eigenvalue sums. The eigenvalue sum is the sum of the energies of all of the occupied states. The eigenvalue sum is more easily calculated, is much smaller than the total energy, and the calculation need not be self-consistent. The calculation shown in Fig. 7 used the force theorem.

In a real sense, the “derivation” of the asymptotic form for the interlayer exchange coupling is based on the force theorem. The energy was assumed to be given as a sum of the energies of all of the occupied electronic states. It turns out that even for realistic systems such an approach can be a reasonable approximation.

Having reduced the interlayer exchange coupling to eigenvalue sums, it is possible to derive the asymptotic formula, Eq. (8) for realistic multilayers [35,36]. This form is derived by ignoring the energy and wave vector dependence of the reflection amplitudes. In the thick limit, including the energy and wave vector dependence leads to contributions higher order in $1/D$ called preasymptotic corrections [37,38]. For Co/Cu(100), where these corrections have been studied in detail, they turn out to be quite important. Asymptotically, the strength of the long period coupling is weak, but for thinner layers, the corrections lead to substantial coupling. For the long period coupling, the wave vector dependence of the majority electron reflection amplitude gives the most important correction. On the other hand, the short period coupling is strong for thick layers, but the energy dependence of the phase of the majority reflection amplitude make it weaker for thin layers.

While Fe/Au(100) multilayers have not been analyzed for preasymptotic corrections, there are indications that they might be important. First, the coupling strengths for the short period coupling calculated using the asymptotic formula disagree with the coupling strength extracted from the full calculation. Second, there are differences between the periods expected from the critical spanning vectors of the Fermi surface and those extracted from Fourier transforms of the calculated coupling [30].

2.3.3 Torques and Spin Currents

When the magnetizations of two adjacent layers are not collinear, the interlayer exchange coupling exerts a torque on both, given by the negative deriva-

tive of the energy, Eq. (4), with respect to the relative angle. Some of the first calculations of the interlayer exchange coupling [39,40] proceeded by directly computing the torque between the magnetization directions. Such calculations proceed analogously to the calculation sketched above, but it is necessary to match non-collinear spin states at the interfaces and to take great care in performing the energy integrals. It is interesting that the torque, which like the energy has contributions from all of the occupied states, can be cast in a form that depends only on the properties of the electrons at the Fermi energy.

Since the interlayer exchange coupling is mediated by the electrons in the spacer layer, the torque is as well. The torque is associated with a spin current flowing in the spacer layer carrying angular momentum from one layer to the other. Angular momentum is extracted from one layer, effectively exerting a torque on the magnetization of that layer, and is deposited in the other layer, effectively exerting an opposite torque on the magnetization of second layer. This spin current differs from the spin current of interest in spintronics [41] because it is carried by all of the electrons in the spacer, not the electrons close to the Fermi level. It also exists independent of an applied voltage. Distinguishing spin currents due to quasi-equilibrium interactions and those related to transport [42] is important to understand possible spintronic devices and also current-induced torques [43,44].

3 Measurement of Interlayer Exchange Coupling

3.1 Growth and Disorder

Growing magnetic multilayers to compare measurements with calculations is quite difficult. Calculations are only tractable for systems that are close to ideal, requiring growth of systems equivalently close to ideal. The first requirement is that the lattices of the different materials need to be compatible. For example, when Co grows on Cu it grows pseudomorphically, that is, it adopts the fcc structure of Cu, with a lattice constant that is very close to that of Cu. For a review of growth in this system see [45]. Another pair of metals with identical crystal structures and close lattice constants is Fe and Cr. Both of these pairs of materials can be grown with several different interface orientations. Some of these are shown in Table 1. Unfortunately, these are the only two pairs of materials with such similar crystal structures. The only other pairs that can be grown sufficiently well are Au or Ag and Fe, but only in the (001) interface orientation. It is somewhat surprising that these systems can be grown well because Fe has a body-centered cubic (bcc) structure while Au and Ag have an fcc structure. In addition, the lattice constants are very different. However, it turns out that if the Fe lattice is rotated by

45° around the interface normal, there is very good in-plane lattice match for each of these pairs [46]. If the starting substrates are sufficiently flat, very good growth can be achieved. However, the presence of steps leads to extended defects through the layer because the Au/Fe growth is not pseudomorphic and the layer thicknesses are quite different.

Interpretation of coupling through Cr spacer layers is complicated by the presence of spin density wave antiferromagnetism [47–49]. In bulk Cr, the transition temperature is close to room temperature, the temperature at which most measurements of the coupling are made. In very high quality multilayers, the antiferromagnetism leads to a short period coupling, which is not well described by the model presented in this paper. However, in addition to the short period coupling associated with the antiferromagnetism, there is a long period oscillatory coupling, which appears to be well described by the model presented here. The properties of this long period coupling are given in Table 1.

Unfortunately, the pairs of materials in Table 1 exhausts the systems that are well enough lattice matched to make high quality comparisons between calculations and measurements. When a material is grown on a substrate that is not so well lattice matched, it assumes the in-plane lattice constant of the substrate on which it is deposited for a couple of monolayers. Then, as the thickness of the deposited layers increases, the strain energy associated with its modified lattice structure becomes too large and the film relaxes by introducing dislocations at the interface. Systems that have been studied in addition to those in Table 1 are reviewed in [50,51]. The same quality of growth has not been achieved in these systems as in the systems with much smaller lattice mismatch.

Even when the lattice mismatch is close to zero, real multilayers are still not perfect. The starting substrate is never perfectly flat and the growth is never perfectly layer by layer, so there are always variations in the thickness of the layers, typically called thickness fluctuations. Frequently, the lateral length scales of the thickness fluctuations are in an intermediate regime. The flat terraces are large enough that the ideal coupling is reasonably well defined over each terrace. On the other hand, the terraces are small enough that the magnetizations do not vary significantly on that length scale. In this intermediate regime, the comparison between calculated and measured coupling strengths is improved by averaging over measured variations of the spacer layer thickness. If the coupling for an ideal thickness of n layers of is $J(n)$ and the probability of having a thickness nd for a nominal deposited thickness of D is $P(n, D)$, the effective coupling strength is

$$J(D) = \sum_n P(n, D)J(n) . \quad (9)$$

If the width of the growth front is measured by scanning tunneling microscopy, x-ray diffraction or some other technique, theoretical coupling strengths can be averaged to compare with measured strengths. The curve in Fig. 7 that is a fit to the experimental data includes the effect of the measured thickness fluctuations through Eq. (9). The coupling strengths with the effect of thickness fluctuations removed are given in Table 2.

When the interlayer exchange coupling has rapid oscillations, the measured coupling is rapidly reduced by the thickness fluctuations. When the coupling strength is reduced by orders of magnitude, it is hard to extract meaningful coupling strengths, even if the growth front has been measured. For this reason, it is desirable to grow the sample in a layer-by-layer mode to keep the growth front as narrow as possible. Since layer-by-layer growth is determined by the competition between nucleation of islands and diffusion of deposited adatoms, it tends to require higher substrate temperatures during growth. Unfortunately, higher growth temperatures tend to promote interdiffusion at the interfaces. Interdiffusion, which gives rise to scattering centers, is more difficult to treat theoretically than thickness fluctuations. It also can be more difficult to measure.

Interdiffusion can have an important and counterintuitive effect on the coupling. In the Fe/Cr(100) system, the measured interdiffusion [52–54], is believed [55] to cause the sign reversal in the measured short period coupling [28,56,57]. Extensions of the calculations discussed above for Fe/Au(100) [30], indicate that interdiffusion may be responsible for the difference between the calculated and measured coupling strengths in Table 2. Those values have already been corrected for the measured thickness fluctuations. It is peculiar that the short period coupling strengths agree much better than the long period strengths. Calculations that include interdiffused atoms at the interface indicate that interdiffusion reduces the long period coupling more than the short period. Since the interdiffusion is not measured for this case, it is possible that it explains the remaining discrepancy between theory and experiment.

The choice of substrate plays a large role in the quality of the growth. The best measurements are made on substrates of one of the materials in the multilayer. Iron whiskers, which can be extremely flat [58], and copper single crystals give the best results. However, insulating substrates are necessary if the samples are also to be used for transport measurements. For these substrates, great care is required to get really high quality growth. See [59] and [60] for descriptions of the complexity of growing a Fe/Au multilayer on a GaAs substrate.

One of the key advances that allowed accurate determination of the oscillation periods was the use of wedge-shaped spacer layers, see Fig. 8. Growing wedge samples simply involves moving a shutter between the sample and the evaporator during growth to expose different parts of the sample to differ-

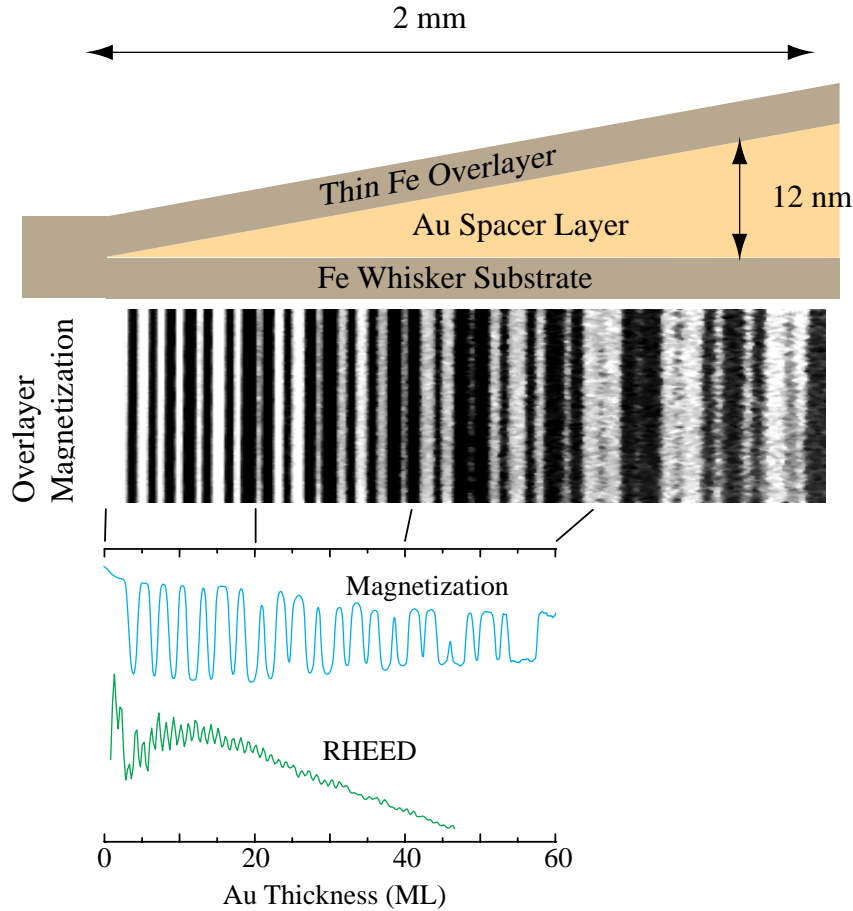


Fig. 8. Interlayer exchange coupling in a wedge shaped Fe/Au/Fe trilayer measured by SEMPA and RHEED [22]. A schematic view of the wedge-shaped sample is shown at the top of the figure. The approximate dimensions give an indication of the very small slope of the wedge. Immediately below is a SEMPA image of the magnetization of the Fe overlayer. White and black indicate parallel and antiparallel alignment to the substrate, and hence ferromagnetic and antiferromagnetic coupling. Below that is a line scan (cyan) through the image and then a measurement of the RHEED intensity (green) along the wedge. The oscillations are used to determine the thickness of the spacer layer along the wedge. The wedge is slightly curved. The RHEED and the magnetization curves have been corrected for this curvature, but the image has not, hence the variation of the lines connecting the image with the line scan.

ent total fluxes. Such samples ensure that all thicknesses are grown under the same conditions because they are grown simultaneously on the same substrate. Wedge samples also make it easier to accurately determine the thickness of the samples.

3.2 Measurement techniques

Measurement of interlayer exchange coupling relies on two broad categories of measurements. One set determines the structure of the multilayer in as much detail as possible. The second determines the magnetic coupling. Common techniques for determining the structure of multilayers are Reflection High Energy Electron Diffraction (RHEED), scanning tunneling microscopy (STM), x-ray scattering, and neutron scattering. Common techniques for determining the coupling are magneto-optical Kerr effect (MOKE), scanning electron microscopy with polarization analysis (SEMPA), Brillouin light scattering (BLS), and ferromagnetic resonance (FMR).

The technique RHEED [61] is commonly used to determine the quality of a surface during growth. A high energy electron beam is reflected from the surface at glancing angles. The resulting diffraction pattern is sensitive to the details of the surface, in particular the presence of steps. If the growth is layer by layer, there are fewer steps when layers are close to complete and more when the layer is half filled. In this case, the intensity of different spots in the RHEED pattern oscillate with a period of one layer. Since the oscillations have a period of a single layer, RHEED oscillations can be used to determine the total thickness of the film. For samples of uniform thickness, RHEED is used to monitor the thickness of the film during growth. For wedge samples, it is typically used after growth, when the RHEED beam is scanned along the wedge and the RHEED oscillations are monitored as a function of position to give the thickness at that position, see Fig. 8.

Techniques used to measure the coupling fall into two broad classes. In the first class, the magnetic configuration is measured, frequently as a function of applied magnetic field. For example, Parkin et al. first observed oscillatory interlayer exchange coupling [10] using the giant magnetoresistance. Here the resistance of the film in zero field was compared with the resistance in large field. If the coupling is ferromagnetic, there is no change, and if the coupling is antiferromagnetic the change can be substantial.

A commonly used technique to determine the magnetic configuration is MOKE [62]. The magneto-optic Kerr effect is the dependence of reflected light on the polarization of the light and the magnetization of the surface. Typically, the polarization of the light rotates through a small angle on reflection. Variations in the rotation can be measured to give the variations in the magnetization that cause them. For wedge samples, MOKE can be used in an imaging mode by scanning the focused spot of a laser across the surface or by imaging a wide area of illumination. It is not particularly surface sensitive and has the advantage that it is sensitive to the magnetic state of both layers. Using the sensitivity to both layers, MOKE images [63] have directly identified perpen-

dicular alignment of two layers, see Section 4. MOKE was used to measure the coupling strengths in Fig 7.

An imaging technique that has been used to determine coupling periods is SEMPA [64]. When a high energy electron beam scatters from a surface, it excites low energy electrons, which leave the surface. These secondary electrons tend to maintain the polarization they had when in the surface. SEMPA measures the magnetization of a region of the sample's surface by determining the polarization of the secondary electrons. Since this technique is based on measuring secondary electrons, which have low energy, it is generally not used with an applied field, limiting it to studies of the remnant state. On the other hand, it has greater spatial resolution than optical techniques like MOKE, and can be used on smaller wedges, requiring smaller areas of sample perfection. Since it can only measure the remnant state, SEMPA has not been used to measure coupling strengths, but it has been used to determine the sign of the coupling for enough oscillations of the coupling to allow high precision measurements of the periods, see Fig. 8. In addition, the electron beam serves as a very high resolution source for measuring RHEED so that both measurements can be done in situ.

When the magnetic state is measured, the interlayer exchange coupling is inferred from the state rather than directly measured. SEMPA images are analyzed with the assumption that the interlayer exchange coupling dominates other energies so that the magnetization points in the direction of the coupling. The MOKE measurements in Fig. 7 are based on images like those shown for SEMPA in Fig. 8, but in the presence of an external applied field. In this case it is assumed that the direction of the coupling is determined by the balance of the interlayer exchange coupling and the interaction with the external field. In both cases, magnetic hysteresis is ignored. Both of the analyses are simple examples of a more general approach. Usually, some magnetic property of a sample, like its hysteresis loop, is measured and the exchange coupling is inferred by comparing the measured property with a model. Some or all of the parameters of the model, including the interlayer layer coupling constant, are varied until the predictions of the model agree with the measurement. The reliability of the results depend on the accuracy of the model, in particular whether it includes all of the physics necessary to describe the experiment.

The second class of measurements used to determine the coupling is based on determining the curvature of the free energy of the magnetization with respect to small variations in the magnetization direction. Two such techniques are FMR and BLS [65]. FMR is based on finding peaks in the microwave absorption of multilayers. The peaks identify resonance frequencies, in other words the frequencies of the uniform modes of a layer. The coupling between the magnetizations of different layers gives rise to coupled oscillations. The different in-phase and out-of-phase resonance frequencies then give the size of

the coupling. BLS is closely related. When light is scattered from the sample, there is a small amount of scattered light that has gained or lost energy by absorbing or exciting a mode of the system. Peaks in the absorption spectrum identify the modes of the system. The mode frequencies can then be analyzed to give the interlayer exchange coupling.

4 Biquadratic Coupling

In almost all multilayers, there is a contribution to the coupling that favors perpendicular alignment of the magnetizations. In many multilayers, this contribution dominates, leading to actual perpendicular alignment of the magnetizations [63,66]. Phenomenologically, this alignment can be explained by a coupling of the form

$$\frac{E}{A} = -J_2(\hat{m}_1 \cdot \hat{m}_2)^2, \quad (10)$$

called biquadratic in contrast to the bilinear coupling discussed above. It is called biquadratic because it is quadratic in both of the magnetization directions. The fact that all measured values of J_2 are negative, favoring perpendicular orientation of the two magnetizations, shows that biquadratic coupling does not have an intrinsic origin similar to the bilinear coupling, but, as Slonczewski showed [67,68], has an extrinsic origin due to disorder.

Thickness fluctuations lead to variations of the coupling strength on different terraces. To lowest order, the intralayer exchange coupling forces the magnetizations in each layer to be uniform so that the bilinear coupling gets averaged over the growth front as described in Eq. (9). To next order, the magnetization can fluctuate around its average direction. Over each terrace, the magnetization fluctuates in the direction that lowers the energy. The fluctuations lower the energy the most when the two magnetizations are perpendicular to each other. This is the origin of the effective interaction favoring perpendicular alignment between the magnetizations.

Consider the simple model shown in Fig. 9, in which the spacer layer consists of parallel strips of width L with alternating thicknesses and hence coupling strengths J^n and J^{n+1} . The relative angle of the magnetizations is $\theta = \theta_0 + \delta\theta \sin(\pi x/L)$, where $\delta\theta$ is the size of the fluctuations. Over the region from 0 to L , where the coupling is J^n , the energy change due to the fluctuations is proportional to $J^n \sin(\theta_0) \delta\theta$. Over the region from L to $2L$, the sine function changes sign and the energy change due to the fluctuations is proportional to $-J^{n+1} \sin(\theta_0) \delta\theta$. The net coupling energy per area due to the fluctuations is proportional to $-\Delta J \sin(\theta_0) \delta\theta$, where $\Delta J = J^n - J^{n+1}$. Fluc-

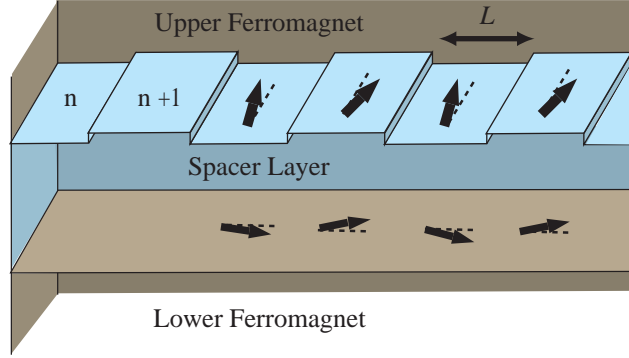


Fig. 9. Thickness variations and biquadratic coupling. The thickness of the spacer layer varies periodically between n and $n + 1$ layers, with ferromagnetic coupling for thicknesses $n + 1$ and antiferromagnetic for thicknesses n . The heavy arrows show the local rotation in the magnetization direction into the direction that minimizes the coupling for each terrace.

tuations in the correct direction lower the energy of the system. The energy gain is balanced by the cost in intralayer exchange energy because the magnetization now varies spatially. Since the intralayer exchange coupling depends on the square of the gradient of the magnetization, for this simple model, it is proportional to $(A_{\text{ex}}/L) \delta\theta^2$, where A_{ex} is the strength of the exchange interaction. Combining the changes due to the fluctuations for the interlayer exchange coupling and the intralayer exchange and finding the minimum with respect to the amplitude of the fluctuations gives $\delta\theta \propto -\sin(\theta_0)\Delta J/(A_{\text{ex}}/L)$. For this fluctuation amplitude, the change in the energy per area due to the fluctuations gives the strength of the biquadratic coupling

$$J_2 \sim -\frac{(\Delta J)^2 L}{A_{\text{ex}}} . \quad (11)$$

While Eq. (11) is quite simple, it qualitatively describes the features of more realistic situations. In real systems, a characteristic length scale L of the arbitrary-shaped terraces replaces the width of the stripes. As this length scale increases, the biquadratic coupling strength increases because the fluctuations can get larger. Also, realistic growth fronts generally consist of more than two thicknesses, which introduces an effective ΔJ . The coupling increases as the difference in the coupling for the different terraces get larger. The differences tend to be largest when the coupling is oscillating rapidly, that is when there is short period coupling. The coupling gets weaker as the intralayer exchange interaction increases because exchange suppresses the fluctuations in magnetization direction that lower the energy.

5 Summary

I have attempted to pedagogically describe interlayer exchange coupling using a simple physical picture that has evolved over the last decade. Spin dependent reflection from the interfaces in multilayers communicates the magnetic state of one ferromagnetic layer through a non-magnetic layer to a neighboring ferromagnetic layer. This communication leads to an exchange interaction between the layers. The exchange interaction has oscillatory contributions with periods determined by the critical spanning vectors of the spacer layer Fermi surface and strengths determined by the spin-dependent reflection at the interfaces.

The oscillations in the exchange interaction arise from the spin-dependent quantum well states set up by the reflection. These quantum well states evolve in energy as the thickness of the spacer layer is varied. As these states pass through the Fermi energy, they fill or empty, changing the energy of the multilayer. These changes are periodic because the quantum well states cross the Fermi energy with a period determined by the Fermi surface of the spacer layer material. At critical points of this Fermi surface, many quantum well states have the same period giving a net oscillatory contribution to the energy. The energy difference between the parallel and antiparallel alignment of the magnetizations gives the interlayer exchange coupling.

The oscillations in the interlayer exchange coupling are analogous to the oscillations in the de Haas-van Alphen effect. The periods of both are determined by critical geometrical properties of the Fermi surface. In fact, the Fermi surface geometries extracted from de Haas-van Alphen experiments can be used to predict the periods of the coupling. The agreement between these periods and the coupling periods, which have been measured to 3 % accuracy in the best cases, provides strong support for our understanding of the coupling.

The periods of the oscillatory interlayer exchange coupling are relatively insensitive to the presence of defects in the multilayer but the coupling strengths are not. The measurements that have been done on defects and the calculations of their effect on the coupling give indications that our understanding of interlayer exchange coupling is correct. Improving our understanding will require measuring the coupling in systems that are as close to perfect as possible and then quantitatively measuring all the defects that remain. The necessary structural characterization will require multiple techniques to measure all of the defects. Then, calculations will need to explicitly treat the measured defects.

The biquadratic coupling that is ubiquitous in magnetic multilayers is an example of an effective interaction that arises because of defects and frustration. Interfacial roughness gives rise to fluctuations in the strength of the bilinear

coupling. The system can lower its energy by allowing the magnetization of the layers to fluctuate in response to the roughness induced variations. The system can lower its energy the most when the two magnetizations are perpendicular to each other, giving an effective coupling that favors perpendicular alignment of the magnetizations.

For more information on interlayer exchange coupling, there are a number of review articles. The series *Ultrathin Magnetic Structures I-IV* consists of review articles on the general topic of magnetic multilayers. Chapter 2 of *Ultrathin Magnetic Structures II* contains four review articles written around 1993 covering various aspects of interlayer exchange coupling [69]. Volume III contains yet another review article, written in 2002. Volume 200 of the *Journal of Magnetism and Magnetic Materials* consists of a series of review articles covering much of magnetism and includes many related to magnetic multilayers. The article on interlayer exchange coupling [50] focuses on the comparison between theory and experiment. Other general review articles on interlayer exchange coupling include [68,70–73]. For a compendium of theoretical and experimental results for specific systems, see [51]. The system Fe/Cr is sufficiently rich that it has generated three review articles on its own [47–49]. Most of the articles above focus on transition metal multilayers, for reviews of rare earth multilayers, see [74,75]. As mentioned above, photoemission studies of quantum well states in magnetic multilayers are reviewed in [16–19]. Biquadratic coupling is reviewed in [76].

References

- [1] W. J. de Haas and P. M. van Alphen, Leiden Comm. 208d (1930); D. Schoenberg, in Proc. 9th Internat. Conf. on Low Temperature Physics, Daunt, Edwards, Milford, Yaquob, ed. Plenum Press, New York, 1965, p.665.
- [2] M. A. Ruderman and C. Kittel, Phys. Rev. **96**, 99 (1954); T. Kasuya, Prog. Theor. Phys. **16**, 45, 58 (1956); K. Yosida, Phys. Rev. **106**, 893 (1957).
- [3] J. C. Bruyere, O. Massenet, R. Montmory, and L. Néel, C. R. Hebd. Seances Acad. Sci. **258**, 841 (1964); *ibid* **258**, 1423 (1964); O. Massenet and R. Montmory, C. R. Hebd. Seances Acad. Sci. **258**, 1752 (1964).
- [4] L. Néel, C. R. Hebd. Seances Acad. Sci. **255**, 1545 (1962); *ibid* **255**, 1676 (1962).
- [5] P. Grünberg, R. Schreiber, Y. Pang, M. B. Brodsky, and H. Sowers, Phys. Rev. Lett. **57**, 2442 (1986).
- [6] C. F. Majkrzak, J. W. Cable, J. Kwo, M. Hong, D. B. McWhan, Y. Yafet, J. V. Waszcak, and C. Vettier, Phys. Rev. Lett. **56**, 2700 (1986).
- [7] M. B. Salamon, S. Sinha, J. J. Rhyne, J. E. Cunningham, R. W. Erwin, J. Borchers, and C. P. Flynn, Phys. Rev. Lett. **56**, 259 (1986).

- [8] M. N. Baibich, J. M. Broto, A. Fert, F. Nguyen Van Dau, F. Petroff, P. Etienne, G. Creuzet, A. Friederich, and J. Chazelas, *Phys. Rev. Lett.* **61**, 2472 (1988);
- [9] G. Binasch, P. Grünberg, F. Saurenbach, and W. Zinn, *Phys. Rev. B* **39**, 4828 (1989).
- [10] S. S. P. Parkin, N. More, and K. P. Roche, *Phys. Rev. Lett.* **64**, 2304 (1990).
- [11] *Electron correlations in molecules and solids*, by P. Fulde (Springer-Verlag, New York, 1995); K. Held, D. Vollhardt *European Phys. J. B* **5**, 473 (1998); I. Yang, S. Y. Savrasov, and G. Kotliar, *Phys. Rev. Lett.* **87**, 216405 (2001).
- [12] W. Kohn and L.J. Sham, *Phys. Rev. A* **140**, 1133 (1965); U. von Barth and L. Hedin, *Phys. Rev. B* **4**, 1629 (1972); O. Gunnarsson and B. I. Lundqvist, *Phys. Rev. B* **13**, 4274 (1976); R. O. Jones and O. Gunnarsson *Rev. Mod. Phys.* **61**, 689 (1989).
- [13] *Calculated electronic properties of metals* by V. L. Moruzzi, J. F. Janak, A. R. Williams (Pergamon, New York, 1978).
- [14] *The Fermi Surface Database*, by T.-S. Choy, J. Naset, J. Chen, S. Hershfield, and C. J. Stanton, <http://www.phys.ufl.edu/fermisurface/>; see also *Fermi Surfaces*, by C. Lehmann, S. Sinning, P. Zahn, H. Wonn, and I. Mertig, <http://www.phy.tu-dresden.de/fermisur/>.
- [15] The earliest calculation of oscillatory coupling in this model actually preceded the discovery of interlayer exchange coupling, A. Bardasis, D. S. Falk, R. A. Ferrell, M. S. Fullenbaum, R. E. Prange, and D. L. Mills, *Phys. Rev. Lett.* **14**, 298 (1965).
- [16] F. J. Himpsel, *Phys. Rev. B* **44**, 5966 (1991). J. E. Ortega and F. J. Himpsel, *Phys. Rev. Lett.* **69**, 844 (1992). J. E. Ortega, F. J. Himpsel, G. J. Mankey, and R. F. Willis, *Phys. Rev. B* **47**, 1540 (1993).
- [17] N. B. Brookes, Y. Chang, and P. D. Johnson, *Phys. Rev. Lett.* **67**, 354 (1991).
- [18] R. K. Kawakami, E. Rotenberg, E. J. Escorcia-Aparicio, H. J. Choi, J. H. Wolfe, N. V. Smith, and Z. Q. Qiu, *Phys. Rev. Lett.* **82**, 4098 (1999).
- [19] Z. Q. Qiu and N. V. Smith *J. Phys. Condens. Matter* **14**, R169 (2002).
- [20] D. M. Edwards, J. Mathon, R. B. Muniz, and M. S. Phan, *Phys. Rev. Lett.* **67**, 493 (1991).
- [21] P. Bruno and C. Chappert, *Phys. Rev. Lett.* **67**, 1602 (1991).
- [22] J. Unguris, R. J. Celotta, and D. T. Pierce, *J. Magn. Magn. Mater.* **127**, 205 (1993).
- [23] J. Unguris, R. J. Celotta, and D. T. Pierce, *J. Appl. Phys.* **75**, 6437 (1994).
- [24] M. T. Johnson, S. T. Purcell, N. W. E. McGee, R. Coehoorn, J. aan de Stegge, and W. Hoving, *Phys. Rev. Lett.* **68**, 2688 (1992).

- [25] W. Weber, R. Allenpach, and A. Bischof, *Europhys. Lett.* **31**, 491 (1995).
- [26] M. D. Stiles, *Phys. Rev. B* **54**, 14679 (1996).
- [27] L. Tsetseris, B. Lee, and Y.-C. Chang, *Phys. Rev. B* **55**, 11586 (1997);
L. Tsetseris, B. Lee, and Y.-C. Chang, *Phys. Rev. B* **56**, R11392 (1997).
- [28] J. Unguris, R. J. Celotta, and D. T. Pierce, *Phys. Rev. Lett.* **67**, 140 (1991).
- [29] E. E. Fullerton, M. J. Conover, J. E. Mattson, C. H. Sowers, and S. D. Bader, *Phys. Rev. B* **48**, 15755 (1993).
- [30] J. Opitz, P. Zahn, J. Binder, I. Mertig, *Phys. Rev. B* **6309**, 4418 (2001).
- [31] J. Unguris, R. J. Celotta, and D. T. Pierce, *Phys. Rev. Lett.* **79**, 2734 (1997).
- [32] N. S. Almeida, D. L. Mills, and M. Teitelman, *Phys. Rev. Lett.* **75**, 733 (1995).
- [33] J. Lindner, C. Rüdtt, E. Kosubek, P. Pouloupoulos, K. Baberschke, P. Blomquist, R. Wäppling, and D. L. Mills, *Phys. Rev. Lett.* **88**, 167206 (2002)
- [34] M. D. Stiles, *J. Appl. Phys.* **79**, 5805 (1996).
- [35] P. Bruno, *J. Magn. Magn. Mater.* **121**, 238 (1993).
- [36] M. D. Stiles, *Phys. Rev. B* **48**, 7238 (1993).
- [37] J. Mathon, M. Villeret, R. B. Muniz, J. d'Albuquerque e Castro, and D. M. Edwards, *Phys. Rev. Lett.* **74**, 3696 (1995); J. Mathon, M. Villeret, A. Umerski, R. B. Muniz, J. d'Albuquerque e Castro, and D. M. Edwards, *Phys. Rev. B* **56**, 11797 (1997).
- [38] P. Bruno, *Eur. Phys. J. B* **11**, 83 (1999).
- [39] J. C. Slonczewski, *Phys. Rev. B* **39**, 69953 (1989).
- [40] J. R. Cullen and K. B. Hathaway, *J. Appl. Phys.* **70**, 5879 (1991).
K. B. Hathaway and J. R. Cullen, *J. Magn. Magn. Mater.* **104-107**, 1840 (1992).
- [41] I. Žutić, J. Fabian, and S. Das Sarma, *Rev. Mod. Phys.* **76**, 323 (2004)
- [42] E. I. Rashba, *Phys. Rev. B* **68**, 241315 (2003).
- [43] J. C. Slonczewski, *J. Magn. Magn. Mater.* **159**, L1 (1996); **195**, L261 (1999).
- [44] L. Berger, *Phys. Rev. B* **54**, 9353 (1996).
- [45] R. F. C. Farrow, *IBM J. Res. Dev.* **42**, 43 (1998).
- [46] A. Fuß, S. Demokritov, P. Grünberg, and W. Zinn, *J. Magn. Magn. Mater.* **103**, L221 (1992).
- [47] D. T. Pierce, J. Unguris, R. J. Celotta, M. D. Stiles, *J. Magn. Magn. Mater.* **200**, 290 (1999).
- [48] H. Zabel, *J. Phys.-Condens. Matter.* **11**, 9303 (1999)

- [49] R. S. Fishman, *J. Phys.-Condens. Matter* **13**, R235 (2001).
- [50] M. D. Stiles, *J. Magn. Magn. Mater.* **200**, 322 (1999).
- [51] D. E. Bürgler, P. Grünberg, S. O. Demokritov, and M. T. Johnson, in *Handbook of Magnetic Materials, Vol. 13*, ed. K. H. J. Buschow (2001).
- [52] A. Davies, J. A. Stroschio, D. T. Pierce, and R. J. Celotta, *Phys. Rev. Lett.* **76**, 4175 (1996).
- [53] D. Venus and B. Heinrich, *Phys. Rev. B* **53**, R1733 (1996).
- [54] R. Pfandzelter, T. Igel, and H. Winter, *Phys. Rev. B* **54**, 4496 (1996).
- [55] M. Freyss, D. Stoeffler, and H. Dreyssé *Phys. Rev. B* **56**, 6047 (1997).
- [56] S. Demokritov, J. A. Wolf, and P. Grünberg, *Europhysics Letters* **15**, 881 (1991).
- [57] S. T. Purcell, W. Folkerts, M. T. Johnson, N. W. E. McGee, K. Jager, J. aan de Stegge, W. B. Zeper, and W. Hoving, *Phys. Rev. Lett.* **67**, 903 (1991).
- [58] J. A. Stroschio and D. T. Pierce, *J. Vac. Sci. Technol. B* **12**, 1783 (1994).
- [59] D. E. Bürgler, C. M. Schmidt, D. M. Schaller, F. Meisinger, R. Hofer, and H.-J. Güntherodt, *Phys. Rev. B* **56**, 4149 (1997).
- [60] T. L. Monchesky, B. Heinrich, R. Urban, K. Myrtle, M. Klaua, and J. Kirschner, *Phys. Rev. B* **60**, 10242 (1999).
- [61] Chapter 5, in *Ultrathin Magnetic Structures I*, edited by J. A. C. Bland and B. Heinrich (Springer-Verlag, Berlin, 1994).
- [62] B. Heinrich and J. F. Cochran, *Adv. Phys.* **42**, 523 (1993); S. D. Bader and J. L. Erskine, Chapter 4, in *Ultrathin Magnetic Structures II*, edited by B. Heinrich and J. A. C. Bland (Springer-Verlag, Berlin, 1994).
- [63] M. Rührig, R. Schäfer, A. Hubert, R. Mosler, J. A. Wolf, S. Demokritov, and P. Grünberg, *Phys. Status Solidi A* **125**, 635 (1991).
- [64] J. Unguris, in *Magnetic Imaging and its Applications to Materials*, ed. by M. de Graef and Y. Zhu, series *Experimental Methods in the Physical Sciences Series*, (Academic Press, 2000); M. R. Scheinfein, J. Unguris, M. H. Kelley, D. T. Pierce, and R. J. Celotta, *Review of Scientific Instruments* **61**(10), 2501-2526 (1990).
- [65] B. Heinrich and J. F. Cochran, *Adv. Phys.* **42**, 523 (1993); B. Heinrich and J. F. Cochran, Chapter 3, in *Ultrathin Magnetic Structures II*, edited by B. Heinrich and J. A. C. Bland (Springer-Verlag, Berlin, 1994); M. Farle, *Rep. Prog. Phys.* **61**, 755 (1998).
- [66] B. Heinrich, J. F. Cochran, M. Kowalewski, J. Kirschner, Z. Celinski, A. S. Arrott, and K. Myrtle, *Phys. Rev. B* **44**, 9348 (1991).
- [67] J. C. Slonczewski, *Phys. Rev. Lett.* **67**, 3172 (1991).

- [68] J. C. Slonczewski, *J. Magn. Magn. Mater.* **150**, 13 (1995).
- [69] K. B. Hathaway, A. Fert, P. Bruno, D. T. Pierce, J. Unguris, R. J. Celotta, and S. S. P. Parkin, Chapter 2, in *Ultrathin Magnetic Structures II*, edited by B. Heinrich and J. A. C. Bland (Springer-Verlag, Berlin, 1994) p. 45.
- [70] Y. Yafet, in *Magnetic Multilayers*, ed. L. H. Bennett and R. E. Watson (World Scientific, Singapore 1994), p. 19.
- [71] A. Fert, P. Grünberg, A. Barthelemy, F. Petroff, and W. Zinn, *J. Magn. Magn. Mater.* **140-144**, 1 (1995).
- [72] B. A. Jones, *IBM J. Res. Dev.* **42**, 25 (1998).
- [73] P. Bruno, *J. Phys.-Condes. Matter* **11**, 9403 (1999).
- [74] C. F. Majkrzak, J. Kwo, M. Hong, Y. Yafet, D. Gibbs, C. L. Chein, and J. Bohr, *Adv. Phys.* **40**, 99 (1991).
- [75] J. J. Rhyne and R. W. Erwin, in *Magnetic Materials*, Vol. 8, ed. K. H. J. Buschow (North-Holland, Elsevier, Amsterdam, 1995) p. 1.
- [76] S. O. Demokritov, *J. Phys. D* **31**, 925 (1998).